ELSEVIER

Chemical Engineering Journal 115 (2005) 51–62

Chemical Engineering Journal

www.elsevier.com/locate/cej

Mathematical analysis of TAP models for porous catalysts

Phungphai Phanawadee [a,*], Monrudee Phongaksorn [b], Nalinee Chaimongkol [a], Attasak Jaree [a], Jumras Limtrakul [c]

[a] *Department of Chemical Engineering, Faculty of Engineering, Kasetsart University, Chatuchak, Bangkok 10900, Thailand*
[b] *Department of Industrial Chemistry, Faculty of Applied Science, King Mongkut's Institute of Technology North Bangkok, Bangsue, Bangkok 10800, Thailand*
[c] *Department of Chemistry, Faculty of Science, Kasetsart University, Chatuchak, Bangkok 10900, Thailand*

Received 12 April 2005; received in revised form 20 September 2005; accepted 23 September 2005

Abstract

The mathematical models for porous catalysts involving interparticle and intraparticle Knudsen diffusion with and without a first order irreversible reaction in a TAP reactor during a single pulse experiment were analyzed. If the ratio of the interparticle to the intraparticle transport characteristic times (γ) is sufficiently large, the intraparticle concentration distribution follows an intraparticle pseudo-steady state (IPSS) condition. For a three-equal-zone reactor, the IPSS assumption is valid when $\gamma \geq 12.5$, corresponding to a macro-porous domain. For $\gamma < 12.5$, the validity of the IPSS assumption depends on the magnitude of the effectiveness factor. The expressions for the valid domain are proposed. The validity of the IPSS assumption for a thin-zone reactor is also discussed. Moment analysis shows that analytical expressions for the gas conversion are the same for the cases with and without application of the IPSS assumption. The conversion expressions for different shapes of catalyst pellets and different reactor configurations are reported.

Keywords: Temporal analysis of products; TAP reactor; Catalysis; Transient response; Kinetics; Mathematical modeling

1. Introduction

Temporal analysis of products or TAP [1,2] has been recognized as an important transient experimental method for heterogeneous catalytic reaction studies [3]. The experiment is performed by injecting a narrow gas pulse into an evacuated microreactor packed with solid particles. Generally, a TAP pulse response experiment involves injecting a very small amount of gas per pulse. As a result, the pressure rise in the microreactor is small, and gas molecules move through the reactor by Knudsen diffusion. The time-dependent exit flow rate of each gas is detected by a mass spectrometer. A very important feature of the TAP experiment is the very small number of reactant gas molecules compared to the number of active sites of the solid catalyst, and consequently during one pulse the catalyst is not perturbed or changed. This type of experiments is called a single pulse experiment. However, a series of pulses of the reactant gas can change the catalyst composition or structure gradually. The gradual change is monitored by the change in the exit flow rates of reactant and/or product gases. The experiment that involves a series of pulses and gradual change of the catalyst is called a multipulse experiment, which is actually a sequence of single pulse experiments.

The simplest TAP microreactor is a one-zone reactor, which is uniformly packed with inert or catalyst particles. A more common reactor is a three-zone reactor in which the catalyst zone is sandwiched between inert zones. The main advantage of a three-zone reactor is that the temperature distribution in the catalyst zone is more uniform. A three-zone reactor in which the catalyst zone is very thin compared to the length of the reactor is called a thin-zone reactor [4,5]. An advantage of this reactor configuration is the uniform gas concentration distribution in the catalyst zone during a one-pulse experiment and a uniform change in the catalyst composition during a multipulse experiment. Numerical analysis for the non-porous catalyst case has shown that the uniformity can be achieved for practical thickness of the catalyst zone [6].

Interpretation of TAP response data including transport and kinetic parameter estimation requires mathematical models that describe the processes in the reactor. Parameter estimation can

* Corresponding author. Tel.: +662 579 2083; fax: +662 561 4621.
E-mail address: fengphi@ku.ac.th (P. Phanawadee).

1385-8947/$ – see front matter © 2005 Elsevier B.V. All rights reserved.
doi:10.1016/j.cej.2005.09.010

Nomenclature

A cross-sectional area of the reactor (m^2)
C_b interparticle gas concentration (mol/m^3)
$C_{b,IPSS}$ interparticle gas concentration calculated from the IPSS model (mol/m^3)
C_b^* dimensionless interparticle gas concentration, defined by $C_b^* = \frac{C_b}{N_p/\varepsilon_b AL}$
C_p intraparticle gas concentration (mol/m^3)
C_p^* dimensionless intraparticle gas concentration, defined by $C_p^* = \frac{C_p}{N_p/\varepsilon_p(1-\varepsilon_b)AL}$
$C^*_{p(avg)}$ spatial averaged intraparticle gas concentration (dimensionless)
$C^*_{p(avg),IPSS}$ spatial averaged intraparticle gas concentration calculated from the IPSS model (dimensionless)
d_{pellet} pellet diameter (m)
d_{pore} pore diameter (m)
D_b effective Knudsen diffusivity in the interparticle void (m^2/s)
$D_{b,cat}$ effective Knudsen diffusivity in the interparticle void of the catalyst zone (m^2/s)
$D_{b,2}$ effective Knudsen diffusivity in the interparticle void of the second inert zone (m^2/s)
D_p effective Knudsen diffusivity in the intraparticle void (m^2/s)
F exit flow rate (mol/s)
F^* dimensionless exit flow rate, defined by $F^* = \frac{F\varepsilon_b L^2}{N_p D_b}$
I_0 modified Bessel function of the first kind of order zero
I_1 modified Bessel function of the first kind of order one
k adsorption or reaction rate constant (m^3 of gas/mol s)
L length of the reactor (m)
L_{cat} length of the catalyst zone (m)
L_e effective length of the catalyst pellet
L_2 length of the second inert zone (third zone in a three-zone reactor) (m)
m_j j^{th} moment of the dimensionless exit flow rate, defined by Eq. (12)
m_0 zeroth moment of the dimensionless exit flow rate
m_1 first moment of the dimensionless exit flow rate
m_2 second moment of the dimensionless exit flow rate
M_T Thiele modulus
M molecular weight
N_p number of moles of gas in the inlet pulse (mol)
r radial coordinate of the pellet (m)
$\bar{r}$ average radius of a void volume (m)
R gas constant (J/mol K)
R_p radius of the catalyst pellet (m)
s variable of Laplace transformation (1/s)
t time (s)
t_{res} mean residence time of the gas exiting the reactor (s)
T temperature (K)
X conversion of the reactant
z axial coordinate of the reactor (m)

Greek letters

α dimensionless reactor parameter, defined by $\alpha = \frac{D_{b,cat}L_2}{D_{b,2}L_{cat}}$
β ratio of intraparticle to interparticle void volumes $\beta = \frac{\varepsilon_p(1-\varepsilon_b)}{\varepsilon_b}$
γ ratio of the interparticle to the intraparticle transport characteristic times defined by Eq. (3)
$\delta(\xi - 0^+)$ Dirac delta function placed at $\xi = 0^+$
$\delta(\tau - 0^+)$ Dirac delta function placed at $\tau = 0^+$
ΔC_{avg} percentage difference in the averaged intraparticle concentrations, defined by $\Delta C_{avg} = \frac{C^*_{p(avg),IPSS} - C^*_{p(avg)}}{C^*_{p(avg)}} \times 100$
ΔC_s percentage difference in the concentrations at the external surface of the catalyst pellet, defined by $\Delta C_s = \frac{C_{b,IPSS} - C_b}{C_b} \times 100$
ε fractional voidage
ε_b interparticle fractional voidage
$\varepsilon_{b,cat}$ interparticle fractional voidage of the catalyst zone
ε_p intraparticle fractional voidage
η effectiveness factor
κ dimensionless adsorption/reaction rate constant, defined by $\kappa = \frac{k\rho_s\varepsilon_{b,cat}L^2}{\varepsilon_p D_{b,cat}}$
ξ dimensionless axial coordinate, defined by $\xi = \frac{z}{L}$
ρ dimensionless radial coordinate
ρ_s concentration of active site, mol/m^3 of the catalyst pellet
τ dimensionless time, defined by $\tau = tD_b/\varepsilon_b L^2$
τ_p peak time of the dimensionless exit flow rate
τ_{res} dimensionless mean residence time, defined by $\tau_{res} = \frac{t_{res}D_b}{\varepsilon_b L^2}$
τ' tortuosity factor
τ'_{inter} interparticle tortuosity factor
τ'_{intra} intraparticle tortuosity factor
ψ dimensionless kinetic parameter, defined by $\psi = \frac{k\rho_s(1-\varepsilon_{b,cat})L^2_{cat}}{D_{b,cat}}$

be accomplished by curve fitting between the experimental exit flow rate and the model exit flow rate calculated from an analytical solution or by a numerical method. Another alternative is the use of moment analysis of the exit flow rate.

Analytical solutions and moment expressions for the exit flow rates can be determined for a one-zone reactor when the models are described by linear differential equations, and uniform temperature and surface concentration distributions are assumed. Analytical solutions for the exit flow rate of a gas from a one-zone reactor packed with non-porous catalyst pellets for simple

processes, i.e., diffusion, diffusion with irreversible adsorption/reaction or with reversible adsorption, have been reported [1,2,7]. Moment expressions for the exit flow rate for those cases were also determined [1,2,7,8]. For a three-zone reactor, no analytical solution for the exit flow rate has been reported. However, moment expressions for the exit flow rate, i.e., first moment for diffusion case [9], zeroth moment for diffusion with irreversible adsorption/reaction case [10–12], first and second moments for diffusion with a reversible adsorption/reaction [13] were reported. For a thin-zone reactor, the zeroth moment expressions for diffusion with irreversible adsorption/reaction and diffusion with reversible adsorption are much simpler [4,12].

Those mentioned theoretical works are related to non-porous catalysts. Industrial catalysts are generally porous, and the TAP experiment has been used to investigate porous catalysts by many research groups [14–24]. When the pore size is considerably larger than the size of the gas molecules, the intraparticle gas transport is described by Knudsen diffusion. The mathematical model involving interparticle and intraparticle Knudsen transport in a TAP reactor was first used by Zou et al. [25] in their simulation work. A simplified model has been proposed by Huinink et al. [26] for the case in which the interparticle diffusion characteristic time is much larger than the intraparticle diffusion characteristic time. A lumped effective Knudsen diffusivity in a bed of porous catalyst pellets which is equal to the interparticle diffusivity times the ratio of the interparticle void volume to the total (intraparticle + interparticle) void volume has been used to describe the transport in the catalyst bed. In fact, this is the case in which a uniform intraparticle concentration distribution is assumed. Analytical solutions for the flow rate of a gas exiting a one-zone reactor were reported for diffusion-only and diffusion with irreversible reaction cases. Diffusion experimental responses from beds of γ-Al_2O_3 (meso-porous) and Li/Sn/MgO (macro-porous) were shown to agree with the analytical solution. However, the magnitude of the ratio of the interparticle to intraparticle diffusion characteristic times that is consistent with the assumption of uniform intraparticle concentration distribution has not been clarified. For diffusion with irreversible reaction case, a criterion for the validity of the simplified model has also been proposed. The lumped diffusivity has been used to describe the interparticle transport combined with intraparticle transport in silica–alumina pores, which was loaded with zeolite [14,22]. A similar catalytic system has been studied using a more complicated model, which includes three different diffusion regimes, i.e., interparticle region, silica–alumina meso-pores, and zeolite micropores [27]. By curve fitting of the exit flow rates, it was shown that the characteristic times in the meso-pores and micropores changed by the degree of coke deposition.

Moment expressions for the exit flow rate in a one-zone reactor have been reported for diffusion-only case by Colaris et al. [28]. It was proposed that the third moment is more reliable to determine the intraparticle diffusivity. The experimental window for using this method was proposed. This window corresponds to the small ratio of the interparticle to the intraparticle characteristic times.Generally, one would like to interpret the experimental responses from a porous system using simple models or methods. A non-porous assumption has been applied to meso-porous [29] and macro-porous [11,15,30] systems. It is not clear whether the non-porous assumption is valid. In fact, how the intraparticle gas concentration distribution evolves during a TAP pulse experiment is not well understood. The analysis of the concentration distribution would provide a basic knowledge that can lead to a proper simplified model.

In this paper, the primary model for spherical porous catalysts involving interparticle and intraparticle Knudsen diffusion with and without a first order irreversible reaction in a TAP reactor during a single pulse experiment is analyzed using a dimensionless form. The gas concentration distribution in the catalyst pellet is examined instantaneously in meso- and macro-porous domains indicated by the magnitude of the ratio of the interparticle to the intraparticle transport characteristic times. It will be shown that when this ratio is sufficiently large, the gas concentration profiles in the pellet follow an intraparticle pseudo-steady state (IPSS) condition. The domain of the parameters in which the IPSS assumption is valid will be discussed. Besides, analytical expressions for the zeroth moment of the exit flow rate and the gas conversion for different shapes of the catalyst pellets and different reactor configurations will be reported. The expressions provide a method to estimate the irreversible reaction rate constant without any simplification of the model. In addition, these expressions will indicate whether the non-porous assumption is valid.

2. Primary mathematical model

The primary model for the first order irreversible adsorption/reaction during a single pulse experiment with spherical porous catalyst pellets is analyzed. When assuming that the external surface area of the catalyst is very small and the reaction occurs only in the catalyst pores, the dimensionless mass balance equations for a reactant gas in the catalyst bed, either in a one-zone reactor or in the middle zone of a three-zone reactor, are described by

Interparticle void region:

$$\frac{\partial C_{\mathrm{b}}^*}{\partial \tau} = \frac{\partial^2 C_{\mathrm{b}}^*}{\partial \xi^2} - 3\gamma \left.\frac{\partial C_{\mathrm{p}}^*}{\partial \rho}\right|_{\rho=1} \tag{1}$$

Intraparticle void region:

$$\frac{\partial C_{\mathrm{p}}^*}{\partial \tau} = \gamma \left[\frac{\partial^2 C_{\mathrm{p}}^*}{\partial \rho^2} + \frac{2}{\rho}\frac{\partial C_{\mathrm{p}}^*}{\partial \rho}\right] - \kappa C_{\mathrm{p}}^* \tag{2}$$

The definition of the variables and parameters is given in the nomenclature. These equations contain two parameters, i.e., γ and κ. The parameter γ is the ratio of the interparticle to the intraparticle transport characteristic times:

$$\gamma = \frac{\frac{L^2 \varepsilon_{\mathrm{b}}}{D_{\mathrm{b}}}}{\frac{R_{\mathrm{p}}^2 \varepsilon_{\mathrm{p}}}{D_{\mathrm{p}}}} \tag{3}$$

This parameter plays an important role on the characteristics of the system. The parameter κ is the ratio of the rate constant to the interparticle transport characteristic time.

For a three-zone reactor, assuming that the interparticle gas diffusivity and fractional voidage in all zones are equal, the dimensionless equation for the two inert zones packed with non-porous particles is given by

$$\frac{\partial C_b^*}{\partial \tau} = \frac{\partial^2 C_b^*}{\partial \xi^2} \tag{4}$$

For a one-zone reactor, Eq. (4) is omitted.

The initial and boundary conditions are written in the dimensionless form as

$$0 \le \xi \le 1, \quad \tau = 0, \quad C_b^* = 0 \tag{5}$$

$$0 \le \rho \le 1, \quad \tau = 0, \quad C_p^* = 0 \tag{6}$$

$$\xi = 0, \quad \tau \ge 0, \quad \frac{\partial C_p^*}{\partial \xi} = \delta(\tau - 0^+) \tag{7}$$

$$\xi = 1, \quad \tau \ge 0, \quad C_b^* = 0 \tag{8}$$

$$\rho = 0, \quad \tau \ge 0, \quad \frac{\partial C_p^*}{\partial \rho} = 0 \tag{9}$$

$$\rho = 1, \quad \tau \ge 0, \quad C_p^* = \beta C_b^* \tag{10}$$

The parameter β is the ratio of the intraparticle to the interparticle void volumes. At the boundaries between adjacent zones in the three-zone reactor, continuity of concentrations and flux are applied [31]. In TAP experiments, the measured variable is the exit flow rate. The dimensionless exit flow rate, F^*, is the gradient of the dimensionless gas concentration at the exit and is described by

$$F^* = -\left.\frac{\partial C^*}{\partial \xi}\right|_{\xi=1} \tag{11}$$

The j^{th} moment of the exit flow rate is defined by

$$m_j = \int_0^\infty F^* \tau^j \, \mathrm{d}\tau \tag{12}$$

The analytical expression for the j^{th} moment of the exit flow rate can be determined by the method described in several papers [8,13,32] in which the set of equations were transformed into Laplace domain. The moment expressions can be determined from the Laplace-domain solution for the exit flow rate using

$$m_j = (-1)^j \lim_{s \to 0} \frac{\partial^j F(s)}{\partial s^j} \tag{13}$$

3. Intraparticle pseudo-steady-state model

Primary simulation results showed that when the time is not too small, the shapes of the intraparticle concentration profiles resemble those in steady-state conditions for large γ. Illustrations will be shown in the next section. This is the case in which the accumulation term on the left hand side of Eq. (2) is neglected for sufficiently large γ, and hence an intraparticle pseudo-steady-state (IPSS) can be assumed. Eq. (2) then becomes

$$0 = \gamma \left[\frac{\partial^2 C_p^*}{\partial \rho^2} + \frac{2}{\rho} \frac{\partial C_p^*}{\partial \rho} \right] - \kappa C_p^* \tag{14}$$

Accordingly, the intraparticle gas concentration distribution changes with time but instantaneously follows the pseudo-steady-state condition governed by two boundary conditions, i.e., Eqs. (9) and (10). In other words, the relaxation time in the pore is so short that the intraparticle concentration distribution can be described by the pseudo-steady-state condition. For diffusion-only case ($\kappa = 0$), the distribution of the intraparticle concentration is uniform.

When the IPSS assumption is applied, the mass-balance Eqs. (1) and (2) can be reduced into one equation. Writing a mass balance for the reactant gas over a thin shell of the bed [33] consisting of both interparticle and intraparticle void regions gives

$$\frac{\partial C_b^*}{\partial \tau} + \frac{\partial C_{p(\text{avg})}^*}{\partial \tau} = \frac{\partial^2 C_b^*}{\partial \xi^2} - \kappa C_{p(\text{avg})}^* \tag{15}$$

The variable $C_{p(\text{avg})}^*$ is the instantaneous spatial averaged concentration in the pore. Applying the IPSS assumption, the concentration distribution can be determined using Eq. (14) with the boundary conditions, Eqs. (9) and (10). The averaged concentration can then be described by

$$C_{p(\text{avg}),\text{IPSS}}^* = \eta \beta C_b^* \tag{16}$$

The parameter η is the typical effectiveness factor in the steady-state condition, and is related to the Thiele modulus, M_T, as [34]

$$\eta = \frac{1}{M_T} \left(\frac{1}{\tanh 3M_T} - \frac{1}{3M_T} \right) \tag{17}$$

where

$$M_T = \frac{\sqrt{\frac{\kappa}{\gamma}}}{3} = \frac{R_p}{3} \sqrt{\frac{k \rho_s}{D_p}} \tag{18}$$

Substituting Eq. (16) in Eq. (15), we obtain the mass balance equation for the IPSS model as

$$(1 + \eta\beta) \frac{\partial C_b^*}{\partial \tau} = \frac{\partial^2 C_b^*}{\partial \xi^2} - \kappa \eta \beta C_b^* \tag{19}$$

Eq. (19) can be solved for C_b^* and F^* without intraparticle boundary conditions, Eqs. (9) and (10). An instantaneous intraparticle concentration profile for a corresponding C_b^* is in accordance with Eq. (14).

4. Numerical method and domain of parameters

Dimensionless exit flow rates and intraparticle concentration profiles calculated from the primary and the IPSS models are compared. Sets of equations for both models were transformed into Laplace domain providing the analytical solutions for the gas concentration as well as the exit flow rate. The numerical

Table 1
Average pore diameters (nm) estimated using Eq. (22) for pellet diameters of 200 and 300 μm, reactor length of 2.54×10^{-2} m, bed fractional voidage of 0.36, and ratio of the interparticle to intraparticle tortuosity factors of 1/3

γ	Average pore diameter (nm)	
	d_{pellet} = 200 μm	d_{pellet} = 300 μm
1	3.5	12
10	35	120

solutions in time domain were then calculated using the inverse discrete Fourier transform via the fast Fourier algorithm [35]. Application of this method for TAP models has been discussed in [13,36].

The domain of parameters used in the calculation was chosen according to the typical conditions found in TAP experiments. The simulation was performed using a one-zone reactor for the diffusion-only case, and a three-zone reactor with all equal zones for the case with reaction. Interparticle diffusivities and bed fractional voidages in all zones in the three-zone reactor were assumed to be the same. The value of β is chosen to be 0.75 corresponding to interparticle fractional voidage (ε_b) of 0.36 (spherical pellet) and intraparticle fractional voidage (ε_p) of 0.42. Simulation results will be shown for γ equal to 1 and 10. How those values of γ correspond to real experiments is discussed here. The interparticle and intraparticle effective diffusivities can be calculated using the expression:

$$D_e = \frac{\varepsilon}{\tau'}\frac{2\bar{r}}{3}\left(\frac{8RT}{\pi M}\right)^{1/2} \tag{20}$$

For the intraparticle void region, the parameter $\bar{r}$is the average radius of the pores. The average radius of the interparticle void region can be calculated using [37]

$$\bar{r} = \frac{2\varepsilon_b}{3(1-\varepsilon_b)}R_p \tag{21}$$

From Eqs. (3), (20), and (21), we can write

$$\gamma = 6\frac{(1-\varepsilon_b)}{\varepsilon_b}\frac{\tau'_{inter}}{\tau'_{intra}}\frac{d_{pore}L^2}{d^3_{pellet}} \tag{22}$$

Table 1 shows values of the average pore diameter, d_{pore}, for pellet diameters of 200 and 300 μm. The calculation was based on the reactor length of 2.54×10^{-2} m, a typical length for a TAP-2 system [2], and the ratio of the interparticle to intraparticle tortuosity factors, $\tau'_{inter}/\tau'_{intra}$, of 1/3. The chosen value of the ratio of the tortuosity factor corresponds to τ'_{inter} of 1.5 for spherical pellets [37] and τ'_{intra} of 4.5, an average of the typical values, which ranges from 2 to 7 [38]. According to the calculation results, the values of γ of 1 and 10 are in the meso- and the macro-porous domains, respectively.

5. Analysis for diffusion-only case

Fig. 1 shows the comparison between the exit flow rates from a one-zone reactor calculated from the primary and the IPSS models for the diffusion-only case with γ equal to 10 and 1.

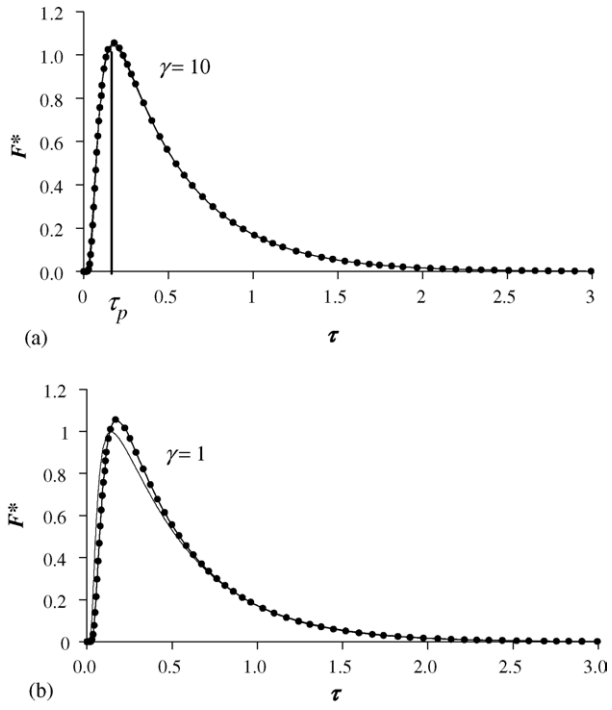

Fig. 1. Exit flow rate curves from a one-zone reactor calculated from the primary (solid line) and the IPSS (circles) diffusion models for γ = 10 and 1.

When γ is as large as 10, the agreement between the two models are excellent. For γ equal to 1, the curve fitting is worse. Fig. 1(a) also shows τ_p, the peak time of the exit flow rate calculated from the primary model. The peak time of each exit flow rate curve is used as a scale for the time period in our analysis.

Fig. 2 shows intraparticle concentration distributions from the two models for $\gamma = 10$ at the middle of the reactor at $\tau = 0.1\tau_p$, $0.5\tau_p$, τ_p, and $4\tau_p$. When time is as small as $0.1\tau_p$, the concentration distributions from the two models are much different. At this time, the concentration distribution from the primary model shows positive gradient indicating the diffusion into the pellet. At $\tau = 0.5\tau_p$, the concentrations from the two models are close to each other especially at $\rho = 1$, the coordinate at the external surface of the pellet.

At larger times as in Fig. 2(c) and (d), the primary model gives negative concentration gradient corresponding to diffusion out off the pellet, and the concentration profiles are very close to those calculated from the IPSS model. Similar characteristics appear at time larger than $4\tau_p$ except that the magnitude is smaller.

The concentration profiles near the inlet at $\xi = 0.1$ and outlet at $\xi = 0.9$ for $\tau = 0.1\tau_p$ and $0.5\tau_p$ are shown in Fig. 3. The diffusion at the position near the inlet is already in the direction out of the pellet, while that near the outlet is still in the reverse direction. The concentration profiles from the two models are fairly close to each other when $\tau = 0.5\tau_p$. An excellent curve fitting is obtained at $\tau = \tau_p$ (not shown here). We also observe that the concentration profiles at the position near the inlet approach IPSS profiles before the position near the outlet.

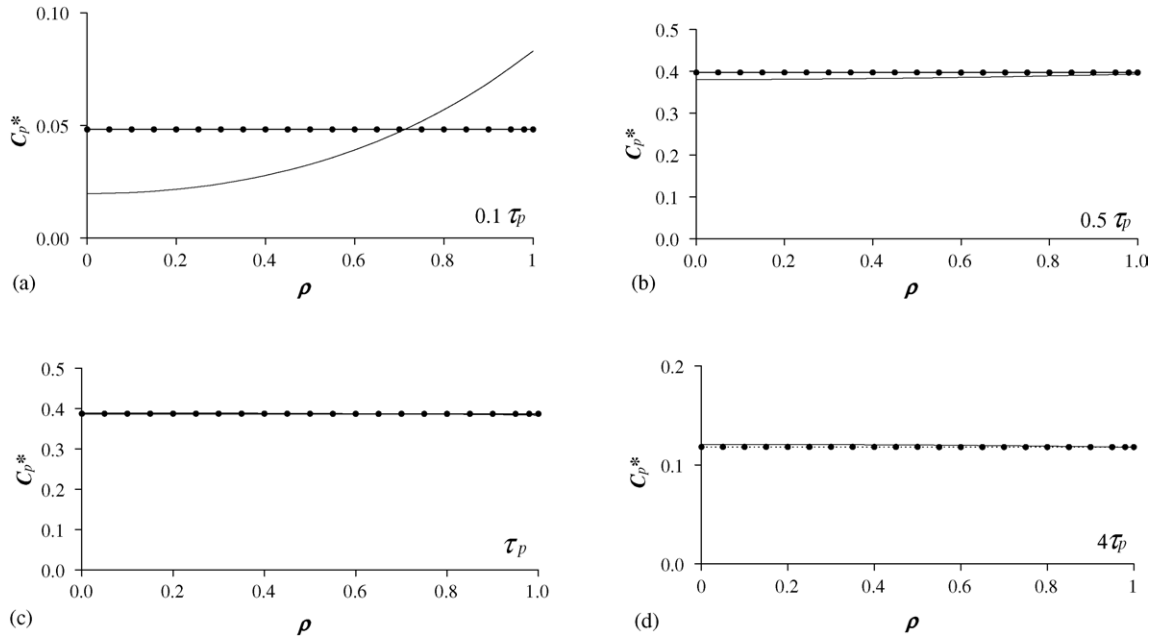

Fig. 2. Concentration profiles in the pellet at the middle of the one-zone reactor calculated from the primary (solid line) and the IPSS (circles) diffusion models for $\gamma = 10$ at different times: $0.1\tau_p$, $0.5\tau_p$, τ_p, and $4\tau_p$.

It has been shown that when γ is as large as 10, the IPSS assumption is excellent based on the exit flow rate curve. Besides, instantaneous concentration profiles in the pellet follow the assumption when time is not too small, i.e., $\tau \geq 0.5\tau_p$. The concentration profiles for $\gamma = 1$ at the middle of the reactor is shown in Fig. 4 for $\tau = 0.5\tau_p$ and $4\tau_p$. Fig. 4(a) and (b) shows that when $\gamma = 1$, the concentration profiles of the two models differ much. However, concentrations at the external surface of the pellet or interparticle concentrations show slight difference. The better agreement of the interparticle concentrations than that of the intraparticle profiles for $\tau \geq 0.5\tau_p$ has also been shown in Figs. 2 and 3. Since the flow rate across the bed is the gradient of the interpartcle concentration, the exit flow rates from both models for $\gamma = 1$ do not differ much (see Fig. 1(b)).

Quantitative comparison between the two models can be given using moment analysis of the exit flow rate. The zeroth moment is unity due to conservation of mass. The first moment

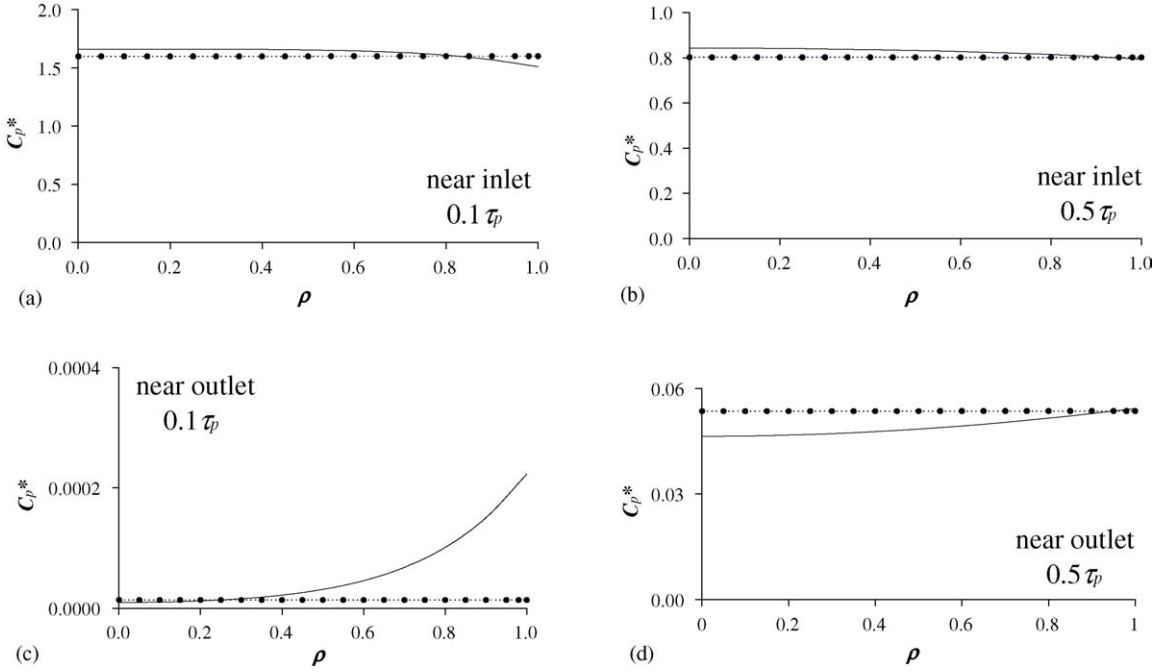

Fig. 3. Concentration profiles in the pellet at the positions near the inlet ($\xi = 0.1$) and outlet ($\xi = 0.9$) of the one-zone reactor calculated from the primary (solid line) and the IPSS (circles) diffusion models for $\gamma = 10$ at $\tau = 0.1\tau_p$ and $0.5\tau_p$.

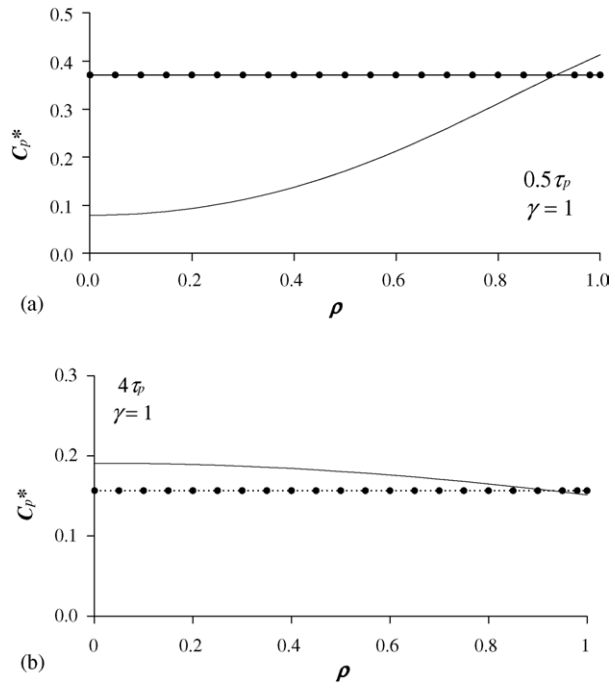

Fig. 4. Concentration profiles in the pellet at the middle of the one-zone reactor calculated from the primary (solid line) and the IPSS (circles) diffusion models for $\gamma = 1$ at $\tau = 0.5\tau_p$ and $4\tau_p$.

and second moment expressions are as followed:

- Both models:

$$m_1 = \frac{1+\beta}{2} \tag{23}$$

- Primary model:

$$m_2 = \frac{5}{12}(1+\beta)^2 + \frac{\beta}{15\gamma} \tag{24}$$

- IPSS model:

$$m_2 = \frac{5}{12}(1+\beta)^2 \tag{25}$$

It is noted that the moment expressions for the primary model have been reported [28] in a different form. The expression for the first moment was found to be the same for both models. As for the second moment, the expression for the primary model contains one term more than the IPSS model, i.e., $\beta/15\gamma$. This term is small when γ is large. For $\beta = 0.75$, the percentage differences of the second moment of the two models are 0.39 and 3.8 for γ equal to 10 and 1, respectively

For the diffusion-only case in a one-zone reactor, the analytical solution for the exit flow is described by

$$F^* = \frac{\pi}{1+\beta}\sum_{n=0}^{\infty}(-1)^n(2n+1)\exp\left[-(n+0.5)^2\pi^2\frac{\tau}{1+\beta}\right] \tag{26}$$

All curves of the IPSS model in Fig. 1 follow Eq. (26). This equation is not limited to the spherical pellet shape as long as the IPSS or a uniform intraparticle concentration distribution is assumed. Huinink et al. [26] has reported Eq. (26) in a dimensional form and experimentally tested with a system of γ-Al_2O_3 pellets with $d_{pellet} = 210$–250 μm, $d_{pore} = 8$ nm, $\varepsilon_p = 0.61$, $\varepsilon_b = 0.48$, and $L = 37$ mm. The result was satisfactory. In this case, when assuming spherical pellets, an estimated value of γ is 2.0, and the corresponding difference of the second moment is only 1.9%. Consequently, the curve fitting is better than that appears in Fig. 1(b).

6. Analysis for irreversible reaction case

Simulation results for the irreversible reaction case in a three-equal-zone reactor is discussed in this section. Fig. 5 compares the exit flow rates calculated from the primary and the IPSS models for different values of κ when γ is equal to 10. The corresponding magnitudes of the effectiveness factor and the conversion are also shown in the figure. The agreement between the two models is excellent throughout the range of the effectiveness factor and the conversion.

For the diffusion-only case ($\kappa = 0$), the characteristics of the concentration distribution in the three-zone reactor are similar to the one-zone reactor. However, since both models involve non-porous inert zones, the effect of the model dissimilarity in the catalyst zone on the exit flow rate is less pronounced. The difference in the second moment is numerically calculated to be 0.18%, which is less than that in the one-zone reactor for the same value of γ.

Fig. 6 shows concentration profiles when the effectiveness factor is equal to 0.5 (corresponding case of Fig. 5(c) at different times and positions in the reactor. The two profiles at the outlet (Fig. 6(c)) differs more than those at the inlet (Fig. 6(a)) and middle (Fig. 6(b)) of the catalyst zone. At $\tau = \tau_p$, an excellent fit is obtained at the outlet as shown in Fig. 6(d).

For the effectiveness factors of 0.94 ($\kappa = 10$) and 0.10 ($\kappa = 8400$), the calculation results are shown in Fig. 7. The latter case, which corresponds to a very large κ, shows excellent curve fitting even at $\tau = 0.1\tau_p$. This is the case in which the kinetic term in Eq. (2) dominates. The profiles at $\tau = 0.1\tau_p$ and $0.5\tau_p$ indicate a very small change in concentration with respect to time. Compared with the diffusion term estimated from the concentration gradient, the accumulation term is much less pronounced. Therefore, the IPSS assumption is more probable.

The simulation results show that it is common to obtain non-uniform concentration distributions in the catalyst pellets even in a macro-porous system. The non-uniform concentration distributions can change the catalyst non-uniformly during a series of pulses, and the apparent kinetic rate constant in one catalyst pellet is then a function of the radial coordinate. The interpretation of TAP responses during a multipulse experiment in this case will then be complicated. The situation is worse when the non-uniformity also occurs along the reactor axial coordinate. The analysis of the uniformity/non-uniformity of the catalyst surface during a multipulse experiment with a porous catalyst will be discussed in a separate article.

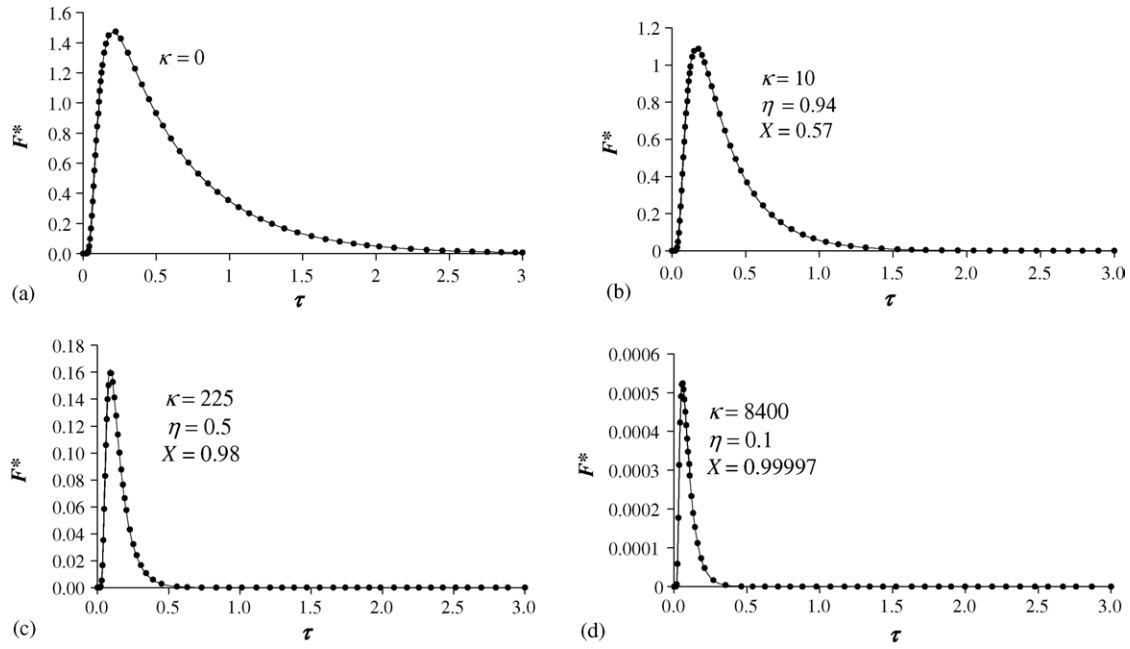

Fig. 5. Exit flow rate curves from a three-equal-zone reactor calculated from the primary (solid line) and the IPSS (circles) models for $\gamma = 10$: (a) $\kappa = 0$, (b) $\kappa = 10$, (c) $\kappa = 225$, (d) $\kappa = 8400$.

Fig. 8 shows the simulation results for $\gamma = 1$ with $\eta = 0.9$. Similarly to the diffusion-only case, the exit flow rates obtained from the two models show good agreement due to the small concentration difference at the external surface of the pellet, but the disagreement in the gas concentration profiles is evident. The results for $\gamma = 1$, $\eta = 0.33$ is shown in Fig. 9. In this case, the agreement in the gas concentration profiles is excellent. The IPSS assumption is shown to be valid for small γ when η is sufficiently small.

7. Validity of the IPSS assumption

The validity of the IPSS assumption was investigated in details. The criterion was chosen so that the small model discrepancy, based on the intraparticle concentration profiles, is obtained for most of the pulse duration. The criterion is as followed:

$$\tau \geq 0.5\tau_p, \quad \left|\Delta C_{avg}\right| \leq 5 \quad \text{and} \quad |\Delta C_s| \leq 10 \tag{27}$$

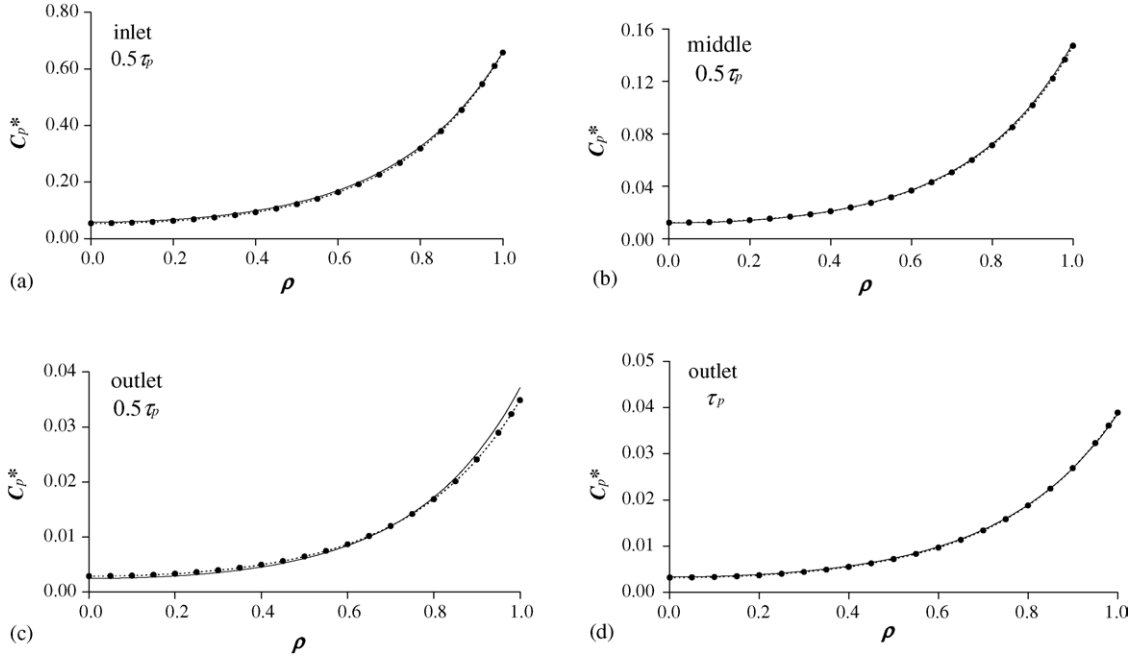

Fig. 6. Intraparticle concentration distributions calculated from the primary (solid line) and the IPSS (circles) models for $\gamma = 10$ and $\kappa = 225$ ($\eta = 0.5$) at different times and positions in a three-equal-zone reactor.

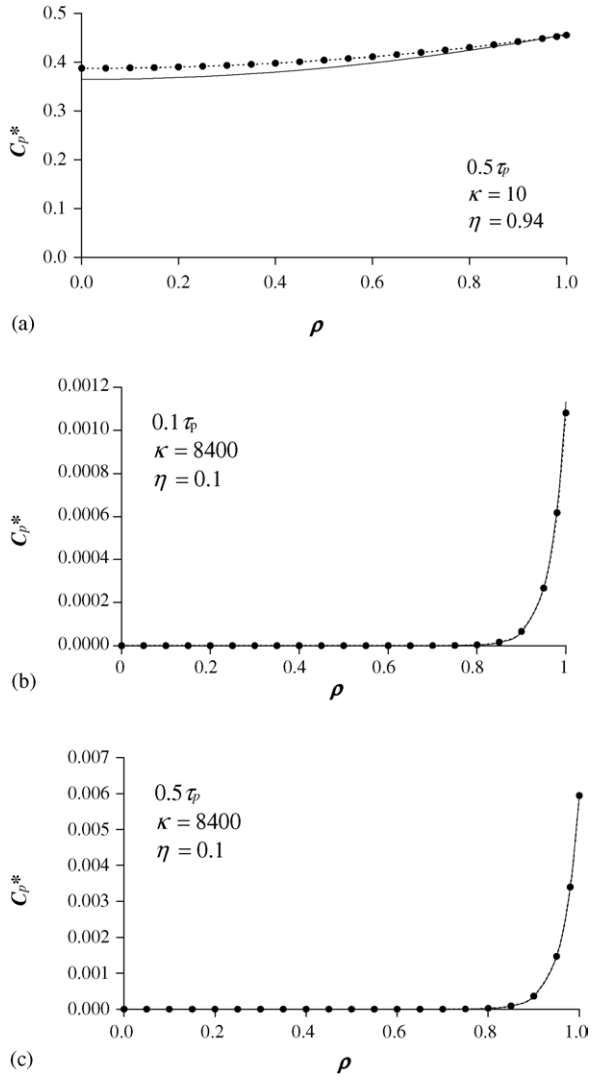

Fig. 7. Intraparticle concentration profiles calculated from the primary (solid line) and the IPSS (circles) models at the middle of the catalyst zone in a three-equal-zone reactor for $\gamma = 10$: (a) $\eta = 0.94$, $\tau = 0.5\tau_p$, (b) $\eta = 0.1$, $\tau = 0.1\tau_p$, (c) $\eta = 0.1$, $\tau = 0.5\tau_p$.

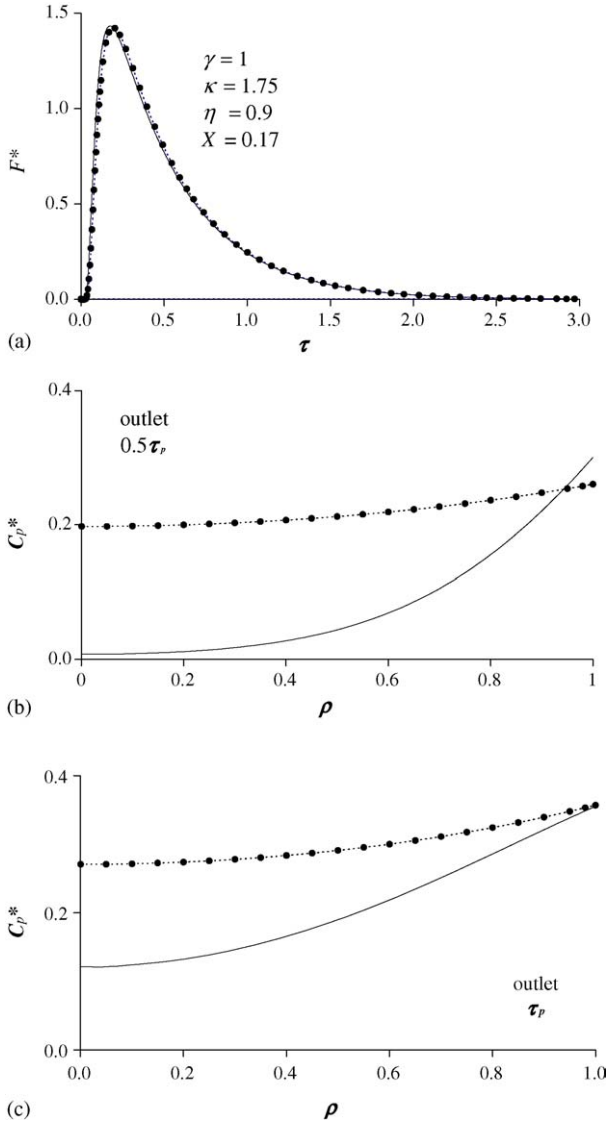

Fig. 8. Comparison of the primary (solid line) and the IPSS (circles) models for a three-equal-zone reactor when $\gamma = 1$, $\kappa = 1.75$, $\eta = 0.9$: (a) exit flow rate curves, (b) intraparticle concentration profiles at the outlet of the catalyst zone at $0.5\tau_p$, (c) intraparticle concentration profiles at τ_p.

The quantity ΔC_{avg} is the percentage difference in the average intraparticle concentrations, and ΔC_s is the percentage difference in the concentrations at the external surface of the catalyst pellet calculated from both models. The requirement for ΔC_s is to exclude circumstances in which the average concentrations are close to each other but the two intraparticle concentration profiles greatly differ from each other. Since the concentration profile at the outlet of the catalyst zone approaches the IPSS profile later than that at the inlet, the detail calculation for the valid region is performed at the outlet of the catalyst zone. Snapshots of intraparticle concentration profiles were compared from $0.5\tau_p$ to the time at which the concentration at the external surface is as small as 1/20 of the corresponding concentration at τ_p. It is noted that all valid cases show excellent agreement at τ_p.

Fig. 10 shows the domain of γ and η within which the IPSS assumption is valid. It is indicated by the region under the dashed line for a three-equal-zone reactor packed with spherical catalyst pellets with $\beta = 0.75$ ($\varepsilon_p = 0.42$; corresponding cases shown in Figs. 5–9). The solid circles show the points obtained from the calculation results. The solid circle at $\gamma = 1$, $\eta = 0.33$ corresponds to the case shown in Fig. 9. The solid circle at $\eta = 1$, $\gamma = 11.1$ refers to the diffusion-only case. When $\gamma \geq 11.1$, the IPSS assumption is valid for the whole range of η. We have also examined the effect of the catalyst porosity on the model discrepancy by varying β from 0.5 to 0.9 (equivalent to changing ε_p from 0.3 to 0.5). The simulation results show that the valid region is most reduced when β is 0.5. The calculation results for $\beta = 0.5$ are shown by the solid triangles. Based on these results, the solid curve is drawn to indicate the valid region for a three-equal-zone reactor with $\beta = 0.5$. The proposed criteria for this valid region are

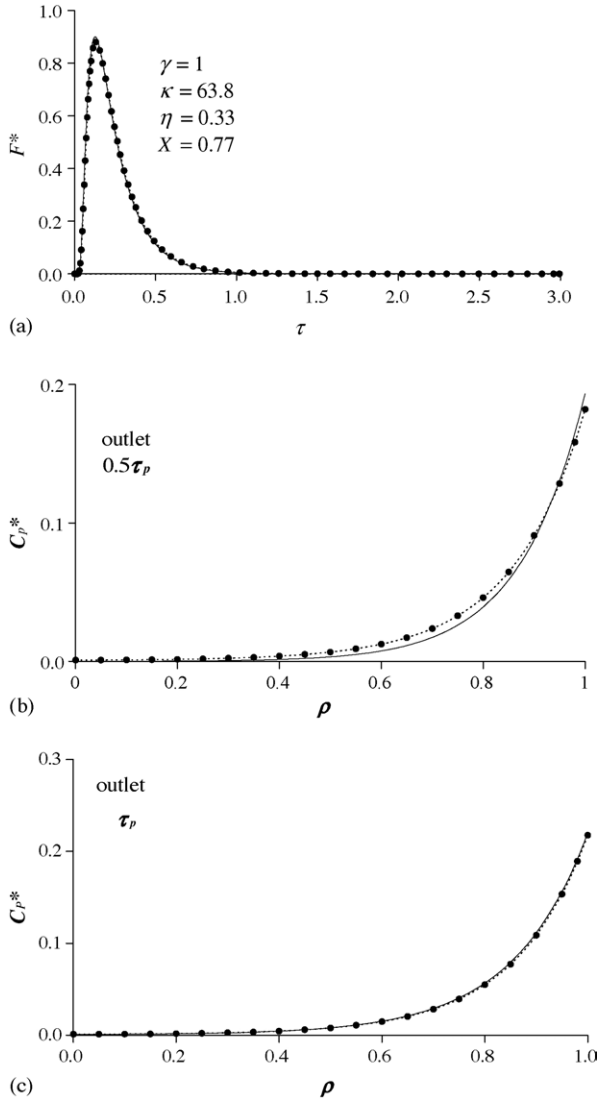

Fig. 9. Comparison of the primary (solid line) and the IPSS (circles) models for a three-equal-zone reactor when $\gamma = 1$, $\kappa = 63.8$, $\eta = 0.33$: (a) exit flow rate curves, (b) intraparticle concentration profiles at the outlet of the catalyst zone at $0.5\tau_p$, (c) intraparticle concentration profiles at τ_p.

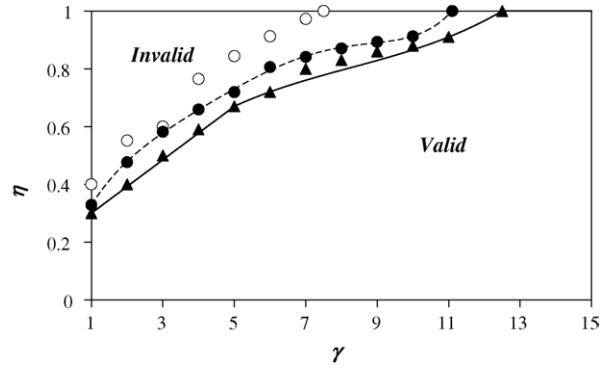

Fig. 10. Domain of γ and η within which the IPSS assumption is valid according to the Eq. (27) for a three-equal-zone reactor with $\beta = 0.75$ (solid circles) and $\beta = 0.5$ (triangles), and for a thin-zone-reactor with $L_{cat}/L = 1/30$ and $\beta = 0.75$ (open circles).

represented as

$$1 \le \gamma \le 5, \quad \eta \le 0.0925\gamma + 0.208, \qquad 5 < \gamma < 12.5,$$
$$\eta \le 0.000718\gamma^3 - 0.0718\gamma^2 + 0.180\gamma + 0.123,$$
$$\gamma \ge 12.5, \quad \text{all } \eta \tag{28}$$

We also compare the valid domains of the IPSS assumption for different lengths of the catalyst zone. The calculation was made for the case in which the length of the catalyst zone (L_{cat}) is decreased to 1/30 of the reactor length (L), a practical configuration for a thin-zone reactor [6], and the catalyst zone is placed in the middle of the reactor. The results are shown by the open circles in Fig. 10 for $\beta = 0.75$. In this case, the valid domain is wider compared with that of the three-equal zone reactor. The decrease in the length of the catalyst zone provides longer distances between the inlets and between the outlets of the catalyst zone and the reactor. This somehow affects the validity of the IPSS assumption. The effect is more evident when the catalyst zone occupies the whole reactor. In this case, the IPSS assumption was tested at $\xi = 0.995$, the position that is very close to the reactor outlet. For the diffusion-only case, the IPSS assumption is valid when $\gamma \ge 9$. When there is an irreversible reaction, it was found that, at this magnitude of γ, the assumption is valid only when $\eta \ge 0.97$. The same domain of η also applies even if the value of γ is three times larger. However, a one-zone reactor is not typically used for reaction studies.

8. Analytical solutions and conversion expressions

For a one-zone reactor when IPSS assumption is applied, the analytical solution for the exit flow rate can be determined by the method of separation of variables. However, the set of the initial and inlet boundary conditions, Eqs. (5) and (7), has to be written in an equivalent form [1,2] as

$$0 \le \xi \le 1, \quad \tau = 0, \quad C_b^* = \delta(\xi - 0^+) \tag{29}$$

$$\xi = 0, \quad \tau \ge 0, \quad \frac{\partial C_b^*}{\partial \xi} = 0 \tag{30}$$

The set of Eqs. (19), (8), (29), and (30) was solved for C_b^*. Then, the solution for the exit flow rate was determined using Eq. (11) and is described by

$$F^* = \frac{\pi}{1+\beta\eta} \exp\left(\frac{-\kappa\beta\eta\tau}{1+\beta\eta}\right) \sum_{n=0}^{\infty} (-1)^n (2n+1) \times \exp\left[-(n+0.5)^2\pi^2 \frac{\tau}{1+\beta\eta}\right] \tag{31}$$

The validity of the IPSS assumption for a one-zone reactor and accordingly Eq. (29) has been discussed in the previous section. If a uniform concentration distribution in the pellet is assumed ($\eta = 1$), Eq. (31) becomes

$$F^* = \frac{\pi}{1+\beta} \exp\left(\frac{-\kappa\beta\tau}{1+\beta}\right) \sum_{n=0}^{\infty} (-1)^n (2n+1) \times \exp\left[-(n+0.5)^2\pi^2 \frac{\tau}{1+\beta}\right] \tag{32}$$

Huinink et al. [26] has reported Eq. (32) and a criterion for the validity, which actually implies a magnitude of the effectiveness factor of 0.99. For the diffusion-only case, Eq. (32) is reduced to Eq. (26).

The mass balance Eq. (19) for the IPSS model has a similar form as that for the non-porous case, and similar simple zeroth moment and conversion expressions for both one- and three-zone reactors can be determined. However, it was found that those expressions for the primary and the IPSS models are unexpectedly the same. For a one-zone reactor, we obtain

$$\text{Both models, one-zone reactor}: \quad m_0 = 1 - X = \frac{1}{\cosh\sqrt{\psi\eta}} \tag{33}$$

The effectiveness factor, η, in Eq. (33) is defined by the same Eqs. (17) and (18) for both models. For a first order irreversible reaction, the effectiveness factor is the ratio of the average concentration in the pellet to the gas concentration at the external surface of the catalyst pellet. The instantaneous η in the primary model therefore changes with time and position according to the intraparticle concentration profiles. Hence, η of the IPSS model is equivalent to the average of η over the whole pulse of the primary model.

The parameter ψ in Eq. (33) is the dimensionless kinetic parameter that appears in a non-porous case [2,8] in which the expression is described by

$$\text{One-zone reactor, non-porous or } \eta = 1: \quad m_0 = 1 - X = \frac{1}{\cosh\sqrt{\psi}} \tag{34}$$

Eq. (34) is good for either the non-porous case or the case in which uniform intraparticle concentration distributions ($\eta = 1$) can be assumed. The difference of the two cases is that the active sites are on the external surface of the catalyst pellets for the non-porous case. The use of the rate constant times the effectiveness factor to calculate conversion via a rigorous expression in TAP transient experiments as shown by Eq. (33) for a one-zone reactor is similar to typical steady state experiments. Similar results were obtained for other reactor configurations.

For a three-zone reactor, the expression is described by

$$\text{Both models, three-zone reactor}: \quad m_0 = 1 - X = \frac{1}{\cosh\sqrt{\psi\eta} + \alpha\sqrt{\psi\eta}\sinh\sqrt{\psi\eta}} \tag{35}$$

If the length of the catalyst zone is very small (a thin-zone reactor), the series for the hyperbolic functions can be truncated, and Eq. (35) becomesThin-zone reactor:

$$m_0 = 1 - X = \frac{1}{1 + \alpha\psi\eta} \tag{36}$$

The validity of Eq. (36) does not depend on η. The domain of α and ψ in which Eq. (36) is a good approximation of Eq. (35) is the same as that reported for the non-porous case [6]. It is noted that Eqs. (35) and (36) are also good for the cases in which the fractional voidages and diffusivities in all zones are not equal.

Eqs. (33), (35), and (36) are not limited to only spherical pellets. It can be proved that those equations can be applied for other pellet shapes when using the same definition of the Thiele modulus described by [34]:

$$M_T = L_e\sqrt{\frac{k\rho_s}{D_p}} \tag{37}$$

The parameter L_e is the effective length that is the volume divided by the external surface area of the catalyst pellet, and for simple shapes we have:

- Flat plates:

$$L_e = \frac{\text{thickness}}{2} \tag{38}$$

- Cylinders:

$$L_e = \frac{R_p}{2} \tag{39}$$

- Spheres:

$$L_e = \frac{R_p}{3} \tag{40}$$

The effectiveness factor for those shapes are as followed:

- Flat plates:

$$\eta = \frac{1}{M_T}\tanh M_T \tag{41}$$

- Cylinders:

$$\eta = \frac{I_1(2M_T)}{M_T I_0(2M_T)} \tag{42}$$

- Spheres: Eq. (17)

Normally, the value of γ is predetermined from the response of an inert gas injected with the reactant gas. Since the diffusivity of a gas is proportional to the reciprocal of the square root of its molecular weight, either the inter- or intraparticle diffusivity of the reactant gas can be calculated from the corresponding diffusivity of the inert gas. However, according to Eq. (3), the magnitude of γ for the inert gas and the reactant gas is the same and is independent of temperature. The parameter γ of an inert gas can be determined using moment expressions [28]. The kinetic parameters can then be determined using the appropriate conversion or zeroth moment expression. The conversion or the zeroth moment can be calculated from the experimental responses of the reactant and the internal standard (inert gas).

The question regarding the validity of the non-porous assumption applied to meso- or macro-porous domains can now be answered. Suppose a one-zone reactor is used, and the non-porous assumption is applied, the magnitude of ψ estimated from Eq. (34) would differ from that in Eq. (33) (for porous model) by a factor of η. This factor also applies to the three- and thin-zone reactors. Therefore, the validity of the non-porous assumption depends on the magnitude of η.

9. Conclusions

The mathematical models for TAP pulse response experiments with porous catalysts for diffusion-only and diffusion combined with a first order irreversible reaction have been analyzed. When $\gamma \geq 12.5$, corresponding to a macro-porous domain, the instantaneous intraparticle concentration profiles in a three-equal-zone reactor follow the IPSS assumption. The expressions for the valid domain have been proposed for $\gamma < 12.5$. This domain also guarantees the IPSS condition for a thin-zone reactor.

The conversion expressions for different TAP reactor configurations and different shapes of catalyst pellets have been reported. The expressions are similar to those for the non-porous case except that the rate constant, ψ, is multiplied by the effectiveness factor. The application of the effectiveness factor for calculating the conversion in transient TAP and typical steady-state experiments is similar.

Acknowledgments

The financial support provided by the senior research scholar fund from the Thailand Research Fund, the National Nanotechnology Center under the National Science and Technology Development Agency, and the Kasetsart University Research and Development Institute is gratefully acknowledged. We also thank Prof. Gregory Yablonsky for many fruitful discussions.

References

[1] J.T. Gleaves, J.R. Ebner, T.C. Kuechler, Catal. Rev. -Sci. Eng. 30 (1988) 49–116.
[2] J.T. Gleaves, G.S. Yablonskii, P. Phanawadee, Y. Schuurman, Appl. Catal. A: Gen. 160 (1997) 55–88.
[3] B.O. Bennett, Adv. Catal. 44 (1999) 329–416.
[4] S.O. Shekhtman, G.S. Yablonsky, S. Chen, J.T. Gleaves, Chem. Eng. Sci. 54 (1999) 4371–4378.
[5] G.S. Yablonsky, S.O. Shekhtman, J.T. Gleaves, S. Chen, Proceedings of the 16th Meeting of the North American Catalysis Society, Boston May 30–June 4, 1999, p. 130.
[6] P. Phanawadee, S.O. Shekhtman, C. Jarungmanorom, G.S. Yablonsky, J.T. Gleaves, Chem. Eng. Sci. 58 (2003) 2215–2227.
[7] J. Huinink, A Quantitative Analysis of Transient Kinetic Experiments: The Oxidation of CO by O_2/NO on Pt. Doctoral Dissertation, Eindhoven University of Technology, The Netherlands. 1995.
[8] G.D. Svoboda, Fundamental Transport-Kinetic Models for Interpretation of TAP Reactor Transient Data with Application to Reactive Systems. Doctoral Dissertation, Washington University, 1993.
[9] P. Phanawadee, G.S. Yablonsky, P. Preechasanongkit, K. Somapa, Ind. Eng. Chem. Res. 38 (1999) 2877–2878.
[10] P. Phanawadee, Theory and Methodology of TAP Knudsen Pulse Response Experiments. Doctoral Dissertation, Washington University, 1997.
[11] O. Dewaele, G.F. Froment, J. Catal. 184 (1999) 499–513.
[12] G.S. Yablonsky, S.O. Shekhtman, P. Phanawadee, J.T. Gleaves, Catal. Today 64 (2001) 227–231.
[13] D. Constales, G.S. Yablonsky, G.B. Marin, J.T. Gleaves, Chem. Eng. Sci. 56 (2001) 133–149.
[14] Y. Schuurman, A. Pantazidis, C. Mirodatos, Chem. Eng. Sci. 54 (1999) 3619–3625.
[15] Y. Schuurman, J.T. Gleaves, Catal. Today 33 (1997) 25–37.
[16] J.H.B.J. Hoebink, J.P. Huinink, G.H. Marin, Appl. Catal. A: Gen. 160 (1997) 139–151.
[17] T. Gerlach, M. Baerns, Chem. Eng. Sci. 54 (1999) 4379–4384.
[18] T.A. Nijhuis, L.J.P. van den Broeke, M.J.G. Linders, J.M. van de Graaf, F. Kapteijn, F. Makke, J.A. Moulijn, Chem. Eng. Sci. 54 (1999) 4423–4436.
[19] C.S. Heneghan, G.J. Hutchings, S.R. O'Leary, S.H. Taylor, V.J. Boyd, I.D. Hudson, Catal. Today 54 (1999) 3–12.
[20] N. Matsui, K. Anzai, N. Akamatsu, K. Nakagawa, N. Ikenaga, T. Suzuki, Appl. Catal. A: Gen. 179 (1999) 247–256.
[21] A. Hinz, A. Andersson, Chem. Eng. Sci. 54 (1999) 4407–4421.
[22] V. Fierro, Y. Schuurman, C. Mirodatos, J.L. Duplan, J. Verstraete, Chem. Eng. J. 90 (2002) 139–147.
[23] J. Aßmann, E. Löffler, A. Birkner, M. Muhler, Catal. Today 85 (2003) 235–249.
[24] C. Breitkopf, J. Mol. Catal. A: Chem. 226 (2005) 269–278.
[25] B.S. Zou, M.P. Dudukovic', P.L. Mills, J. Catal. 145 (1994) 683–696.
[26] J.P. Huinink, J.H.B.J. Hoebink, G.B. Marin, Can. J. Chem. Eng. 74 (1996) 580–585.
[27] Y. Schuurman, C. Delattre, I. Pitault, J.P. Reymond, M. Forissier, Chem. Eng. Sci. 60 (2005) 1007–1017.
[28] A.H. Colaris, J.H.B.J. Hoebink, M.H.J.M. de Croon, J.C. Schouten, AIChE J. 48 (2002) 2587–2596.
[29] O. Dewaele, G.F. Froment, Appl. Catal. A: Gen. 185 (1999) 203–210.
[30] M. Soick, D. Wolf, M. Baerns, Chem. Eng. Sci. 55 (2000) 2875–2882.
[31] B. Zou, M.P. Dudukovic', P.L. Mills, Chem. Eng. Sci. 48 (1993) 2345–2355.
[32] A.S. Anderssen, E.T. White, Chem. Eng. Sci. 26 (1971) 1203–1221.
[33] R.B. Bird, W.E. Stewart, E.N. Lightfoot, Transport Phenomena, Second ed., John Wiley & Sons, New York, 2002.
[34] O. Levenspiel, Chemical Reaction Engineering, Third ed., John Wiley & Sons, New York, 1999, pp. 386–387.
[35] E.O. Brigham, The Fast Fourier Transform and its Applications, Prentice Hall, Englewood Cliffs, New Jersey, 1988.
[36] G.D. Svoboda, J.T. Gleaves, P.L. Mills, Ind. Eng. Chem. Res. 31 (1992) 19–29.
[37] D.G. Huizenga, D.M. Smith, AICHE J. 32 (1986) 1–6.
[38] C.N. Satterfield, Heterogeneous Catalysis in Industrial Practice, Second ed., McGraw-Hill, New York, 1991, p. 501.